analytical chemistry

pubs.acs.org/ac Article

Self-Assembly-Induced Enhancement of Cathodic Electrochemiluminescence of Copper Nanoclusters for a Split-Type Matrix Metalloproteinase 14 Sensing Platform

Xiaoyue Zhang, Yue Jia, Nuo Zhang, Dan Wu, Hongmin Ma, Xiang Ren, Huangxian Ju, and Qin Wei*

Cite This: *Anal. Chem.* 2024, 96, 7265−7273 Read Online

ACCESS | Metrics & More | Article Recommendations | Supporting Information

ABSTRACT: The unique optoelectronic and tunable luminescent characteristics of copper nanoclusters (Cu NCs) make them extremely promising as luminophores. However, the limited luminescence intensity and stability of Cu NCs have restricted their application in the field of electrochemiluminescence (ECL). Herein, a self-assembly-induced enhancement strategy was successfully employed to enhance the cathodic ECL performance of flexible ligand-stabilized Cu NCs. Specifically, Cu NCs form ordered sheetlike structures through intermolecular force. The restriction of ligand torsion in this self-assembled structure leads to a significant improvement in the ECL properties of the Cu NCs. Experimental results demonstrate that the assembled nanoscale Cu NC sheets exhibit an approximately three-fold increase in cathodic ECL emission compared to the dispersed state of Cu NCs. Furthermore, assembled nanoscale Cu NCs sheets were utilized as signal probes in conjunction with a specific short peptide derived from the catalytic structural domain of matrix metalloproteinase 14 (MMP 14) as the identification probe, thereby establishing a split-type ECL sensing platform for the quantification of NMP 14. The investigation has revealed the exceptional performance of assembled nanoscale Cu NCs sheets in ECL analysis, thus positioning them as novel and promising signal probes with significant potential in the field of sensing.

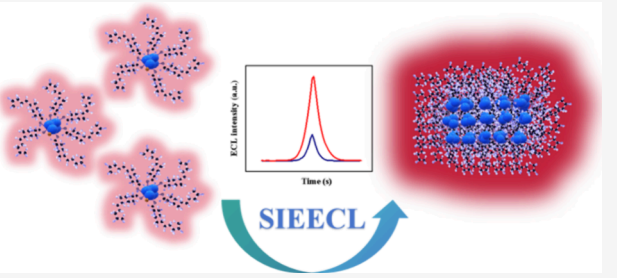

INTRODUCTION

Electrochemiluminescence (ECL) is a phenomenon in which photons are generated through electrochemical reactions.[1] It relies on the redox processes of electrochemical reactions,[2] where electrons or holes are transferred from the electrode to the luminophore in the reaction system at a specific potential, inducing the excited state luminophore to return to its ground state and release photons.[3] As a significant optoelectronic conversion technology, ECL has found extensive applications in various fields such as clinical medicine,[4,5] environmental monitoring,[6,7] and food analysis[8,9] due to its exceptional sensitivity, minimal interference from background signals, and rapid response time.[10] Nevertheless, the exploration of novel luminophores for ECL remains a crucial research focus within this field.[11−13]

The metal nanoclusters (MNCs), consisting of a few to hundreds of metal atoms that are approximately the size of Fermi wavelengths, exhibit distinctive molecular-like properties, rendering them a class of nanomaterials with exceptional optical and electrical characteristics attributed to the quantum size effect.[14] Currently, extensive research has been conducted in the field of ECL with a focus on gold (Au)[15,16] and silver (Ag) NCs.[17,18] However, challenges faced by Au NCs and Ag NCs include relatively high synthesis costs and difficulties in achieving large-scale production. Consequently, copper (Cu) NCs have gradually garnered attention from researchers in the field of ECL.[19,20] Nevertheless, the coordination interaction between ligands coating the surface of Cu NCs and the Cu core can induce ligand-to-metal charge transfer (LMCT) or ligand-to-metal-to-metal charge transfer (LMMCT), resulting in radiative transitions involving the triplet state centered on the Cu core. In this process, factors such as vibrational and rotational motions of the ligands within the molecule results in an increase in the proportion of non-radiative transitions, thereby hindering luminescence intensity enhancement for Cu NCs and limiting their applications in ECL.[21] The concept of self-assembly-induced enhancement in the ECL of Cu NCs offers a novel approach to enhance their ECL performance.[22] By manipulation of the thermodynamic equilibrium among Cu NCs during assembly, densely packed and well-organized two-dimensional (2D) structures can be formed through weak intermolecular interactions. The self-assembled structure effectively mitigates nonradiative transitions caused by intramolecular vibrations or rotations through the coupling of surface ligands, thereby enhancing the ECL performance of Cu NCs.

Received: February 25, 2024
Revised: April 2, 2024
Accepted: April 9, 2024
Published: April 22, 2024

https://doi.org/10.1021/acs.analchem.4c01039
Anal. Chem. 2024, 96, 7265−7273

Scheme 1. Schematic Diagram of the MMP 14 Sensing Platform

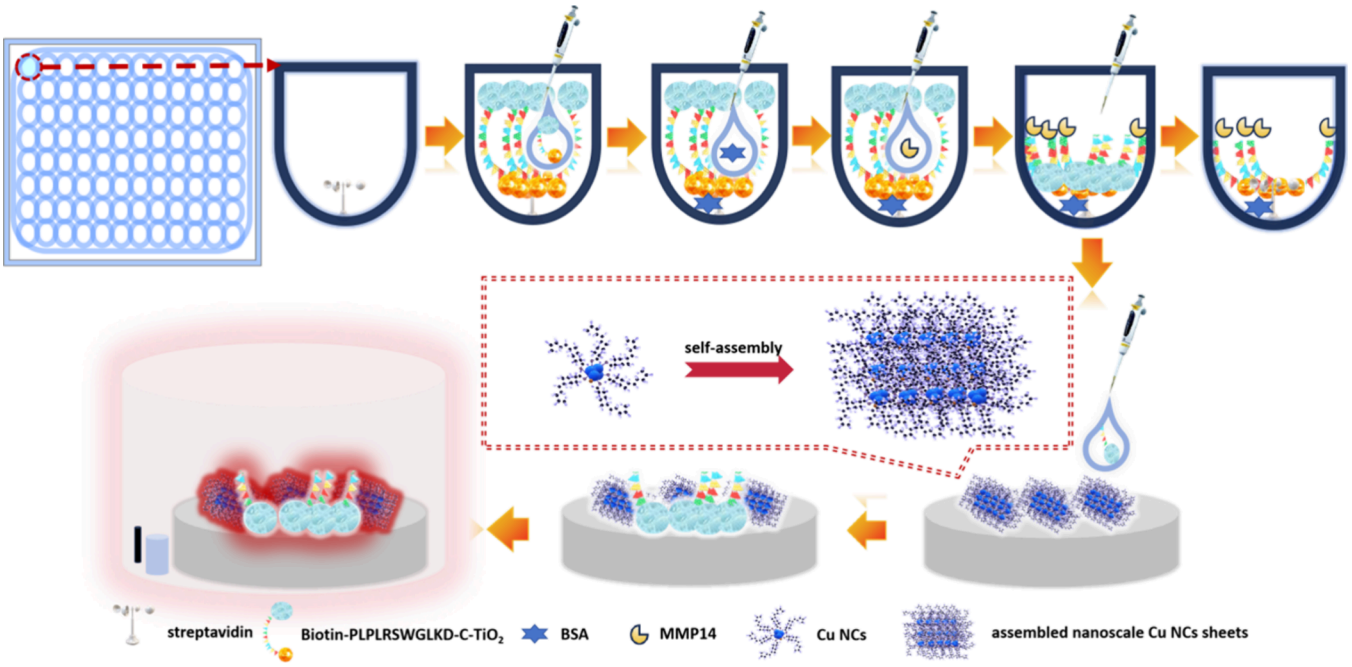

These high-performance Cu NCs can serve as signal probes for sensing platforms.[23]

Matrix metalloproteinases (MMPs) are members of the zinc-dependent endopeptidase family and represent a pivotal group of proteinases with significant implications.[24,25] MMPs play crucial roles in various physiological and pathological processes, including cell migration, tissue repair and remodeling, immune responses, tumor invasion, and metastasis.[26] Aberrant expression of MMPs is closely associated with the onset and progression of diverse diseases, such as inflammatory disorders, cardiovascular conditions, and malignancies.[27,28] Among these enzymes involved in cancer cell penetration through the basement membrane, MMP 14 stands out as a key player whose heightened expression signifies tumor dissemination.[29,30] Currently, there is a lack of research on using ECL-based sensing for MMP 14 detection. Developing a platform for this purpose could be a valuable scientific endeavor, allowing for sensitive detection of MMP 14 at trace levels.

In this work, the flexible ligand dodecanethiol was employed to stabilize Cu NCs, leading to the formation of well-organized sheet-like structures. We conducted a comprehensive investigation of the electrochemical and ECL properties of self-assembled nanoscale Cu NCs sheets as well as their behavior in terms of cathodic ECL enhancement induced by assembly. Leveraging self-assembled nanoscale Cu NCs sheets as signal probes, in conjunction with specifically selected short peptides and nanoscale C-TiO_2, we observed that the introduction of MMP 14 triggered site-specific cleavage of the short peptides, resulting in enhanced sensing signals. The construction of a split-type ECL sensing platform has led to the development of a sensitive detection method for MMP 14.

EXPERIMENTAL SECTION

Reagents and Materials. The Streptavidin-coated 96-well microplates were obtained from BEAVER Biomedical Co., Ltd. Polypeptide chain (Biotin-PLPLRSWGLKD (N−C) was synthesized by Sangon Biotechnology (Shanghai) Co., Ltd. MMP 14 was sourced from DIMA Biotechnology Co., Ltd. Cuprous iodide (CuI) and potassium persulfate ($K_2S_2O_8$) were purchased from Macklin Biochemical Technology Co., Ltd. Dodecanethiol, dibenzyl ether, tetrabutyl titanate, and ethylene glycol were acquired from Aladdin Biochemical Technology Co., Ltd. The MMP 14 ELISA kit was purchased from Tianjin Peptide Chain Biotechnology Co., Ltd. The serum samples were collected from the University of Jinan Hospital with the informed consent of the volunteers and subsequently utilized as test specimens.

Apparatus. The morphology of the Cu NCs in both dispersed and assembled states was characterized by using high-resolution transmission electron microscopy (HRTEM, JEOL). X-ray photoelectron spectroscopy (XPS, Thermo Kalpha) was employed to analyze the element types and valence states of self-assembled nanoscale Cu NCs sheets and C-TiO_2 samples. The crystal structure of C-TiO_2 was determined by X-ray diffractometry (XRD, X'Pert Pro MPD). Infrared spectroscopy (JASCO FTIR-410) was utilized to investigate the infrared absorption behavior of self-assembled nanoscale Cu NCs sheets and C-TiO_2. Optical properties of self-assembled nanoscale Cu NCs sheets were characterized by using a UV−vis spectrometer (PerkinElmer-Lambda 35) and a fluorescence spectrophotometer (PerkinElmer LS-45/55). Relevant ECL measurements were performed on an ECL analyzer (Xi'an Remax). All electrochemical tests were conducted using an electrochemical workstation (Shanghai Chenhua 760e). The Elisa kit was determined using a multifunctional microplate reader (Tecan Spark).

Preparation of the Assembled Nanoscale Cu NC Sheets. Assembled nanoscale Cu NCs sheets were synthesized by the literature method with some modifications.[31] Initially, 38.1 mg of CuI was completely dissolved in 3 mL of dibenzyl ether. Subsequently, 1 mL of dodecanethiol was added, and the mixture was stirred at a constant speed on a hot plate maintained at 70 °C for 30 min, resulting in the formation of a milky white crude product. A volume of 1 mL from the crude product was extracted and subjected to washing by mixing with 1 mL of

https://doi.org/10.1021/acs.analchem.4c01039
Anal. Chem. 2024, 96, 7265−7273

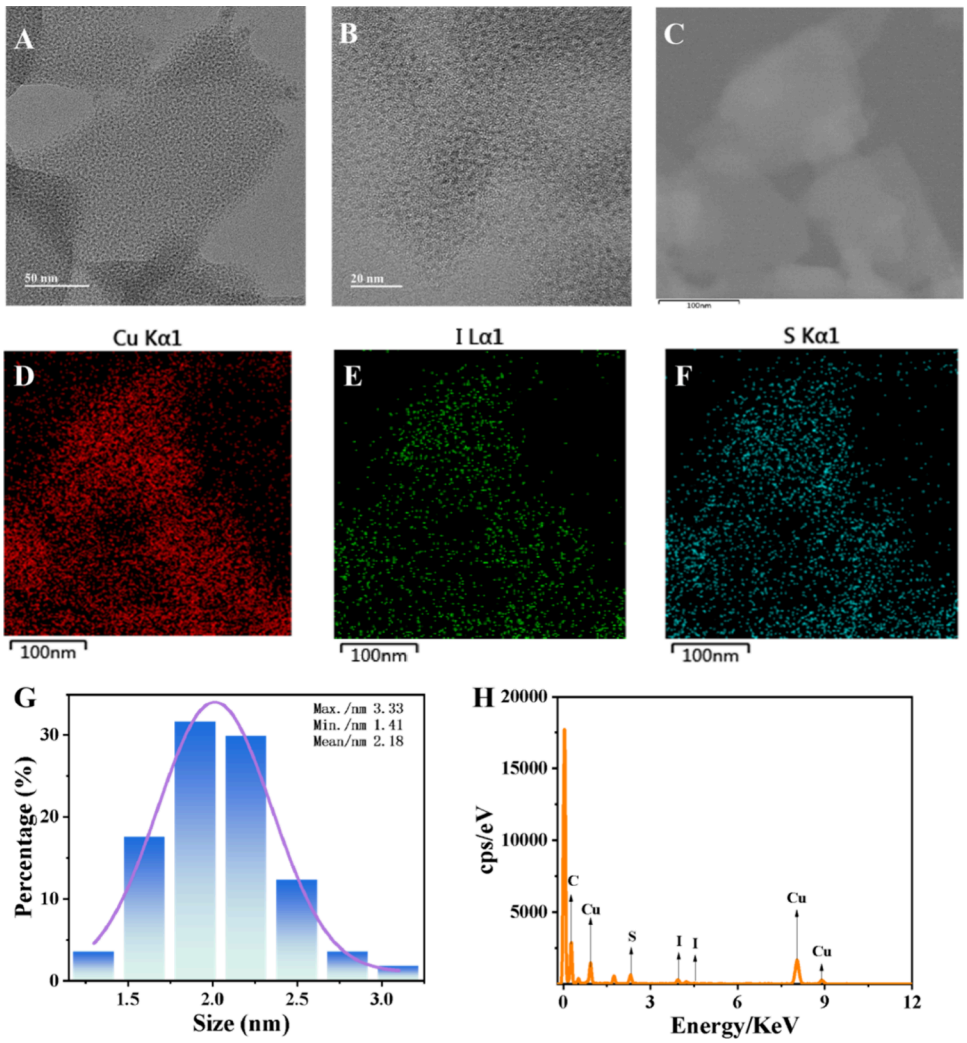

Figure 1. TEM (A), HRTEM (B), and STEM images of assembled nanoscale Cu NCs sheets (C). Cu (D), I (E), and S (F) element mapping images of assembled nanoscale Cu NC sheets. Size distribution of the Cu NCs in the assembled nanoscale Cu NC sheets (G). EDS spectra of assembled nanoscale Cu NCs sheets (H).

chloroform and 2 mL of ethanol, followed by centrifugation at a speed of 7000 rpm for 5 min. The purification steps were repeated three times, after which the precipitate was redispersed in an additional volume comprising 1 mL of chloroform.

Preparation of Biotin-PLPLRSWGLKD-C-TiO_2. The preparation procedure for C-TiO_2 follows a methodology similar to that previously reported.[32] Initially, 1 mL of tetrabutyl titanate was dissolved in 40 mL of ethylene glycol. Subsequently, this solution was gradually added dropwise into 40 mL of deionized water while being stirred for 30 min at ambient temperature. Afterward, the solution underwent transfer into a Teflon-lined autoclave where it underwent reaction for 12 h at a temperature of 180 °C. Upon reaching room temperature through the cooling process, the ultimate precipitate obtained from this reaction was collected and subjected to several rounds of washing/centrifugation using ethanol as well as deionized water. Then, 1000 μL of a 10 mM solution of Biotin-PLPLRSWGLKD was added to a centrifuge tube, followed by the addition of 400 μL of PBS containing 10 mM NHS and 40 mM EDC to activate the COOH groups. The mixture was incubated for 2 h, followed by the addition of 600 μL of C-TiO_2 (6 mg/mL) and overnight reaction at 4 °C. After centrifugation and rinsing with PBS buffer, the Biotin-PLPLRSWGLKD-C-TiO_2 was redispersed and stored in 2 mL of PBS and at 4 °C.

Construction and Testing Process of the Split-Type Sensing Platform. The Biotin-PLPLRSWGLKD-C-TiO_2 was prepared by chilling it on ice, followed by the addition of 100 μL of Biotin-PLPLRSWGLKD-C-TiO_2 to each well of a streptavidin-coated microplate. The microplate was then placed on a horizontal shaker at room temperature and incubated for 1 h. After aspirating the liquid from the wells, 200 μL of PBS was added. The microplate was horizontally shaken for 5 min, followed by the removal of the liquid from the wells. This washing step was repeated three times. Next, each well received 100 μL of PBS containing 5% BSA, and the microplate was incubated at room temperature on a horizontal shaker for 1 h. After aspirating the liquid in the wells, 200 μL of PBS was added and shaken horizontally for another 5 min before removing the supernatant from the wells. This washing step was also repeated three times. Different concentrations of MMP 14 were subsequently added to each well (100 μL each), and then incubated at 37 °C with shaking for 1 h. The liquid from the wells, along with an additional volume of 100 μL PBS washing solution, was collected in centrifuge tubes and thoroughly mixed. Subsequently, a sample volume of 20 μL was extracted

https://doi.org/10.1021/acs.analchem.4c01039
Anal. Chem. 2024, 96, 7265−7273

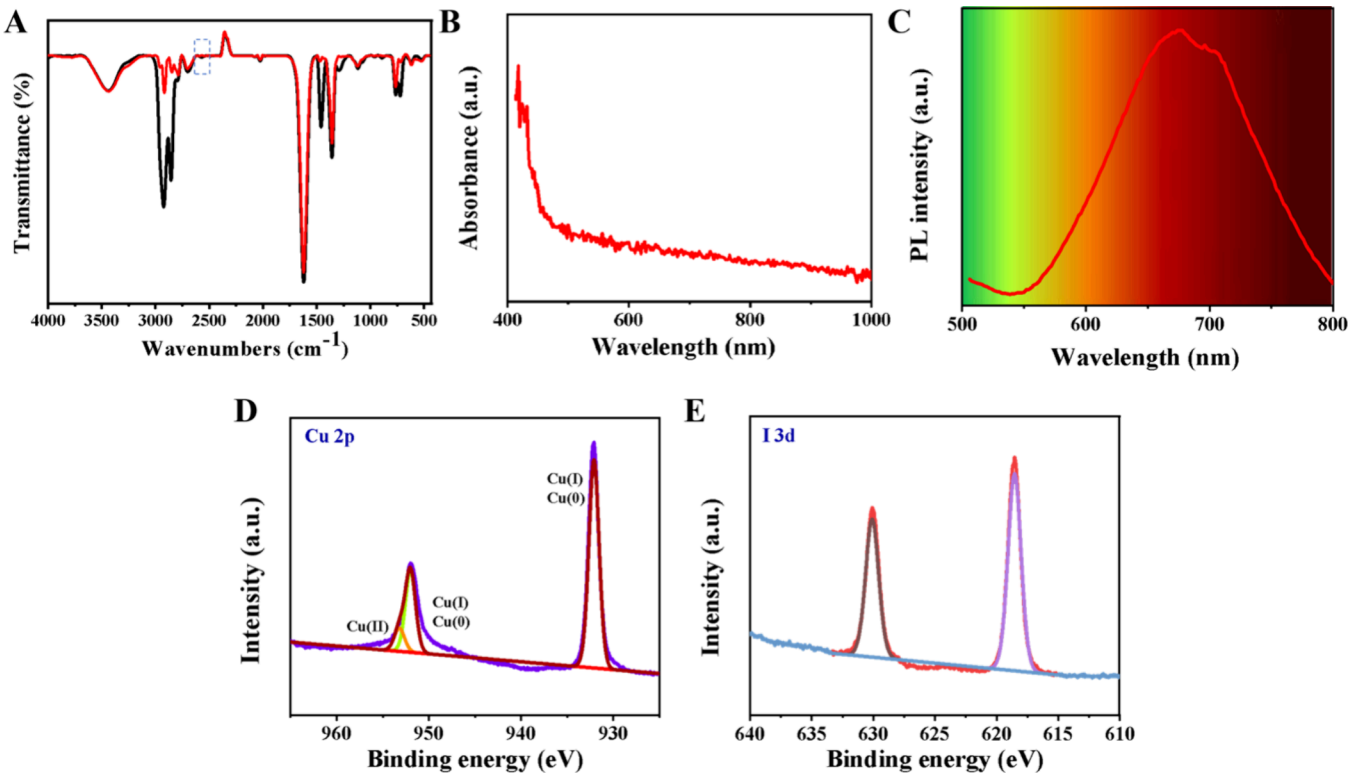

Figure 2. Infrared spectrum of assembled nanoscale Cu NCs sheets (red curve) and dodecanethiol (black curve) (A). UV−vis absorption (B) and PL spectra of assembled nanoscale Cu NCs sheets (C). XPS spectra of Cu 2p (D), I 3d (E) of the assembled nanoscale Cu NCs sheets.

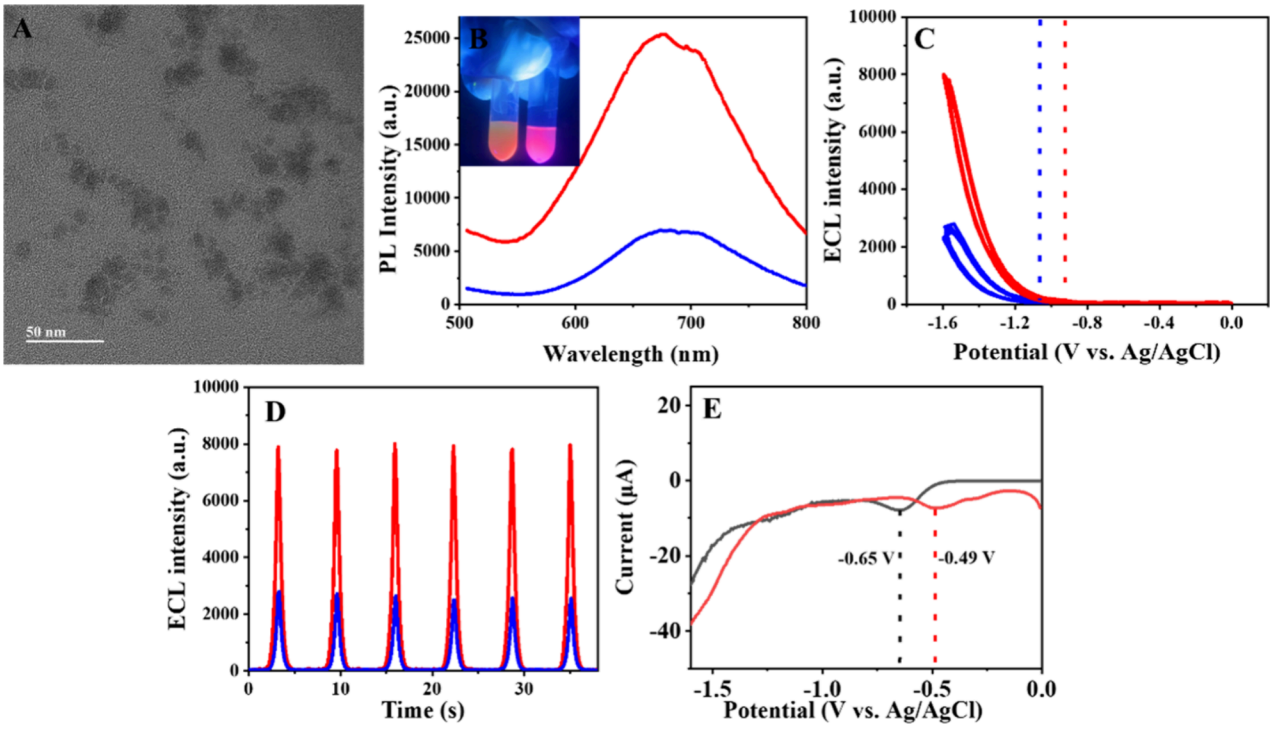

Figure 3. TEM image of dispersed Cu NCs (A). The PL spectra of assembled nanoscale Cu NCs sheets (red curve) and the dispersed Cu NCs (blue curve) with corresponding photographs captured under UV illumination provided as visual representation (inset) (B). ECL-potential curve (C) and ECL-time curve (D) of dispersed Cu NCs (blue curve) and assembled nanoscale Cu NCs sheets (red curve) in 0.1 M pH 7.4 PBS containing 0.1 M $K_2S_2O_8$. DPV curve of dispersed Cu NCs (black curve) and assembled nanoscale Cu NCs sheets (red curve) in 0.1 M pH 7.4 PBS (E).

and dropped onto a glassy carbon electrode (GCE) modified with 5 μL of assembled nanoscale Cu NCs sheets (Scheme 1).

The testing platform utilizes a three-electrode system, in which the modified GCE is the working electrode (WE). Ag/AgCl electrode is employed as the reference electrode (RE),

https://doi.org/10.1021/acs.analchem.4c01039
Anal. Chem. 2024, 96, 7265−7273

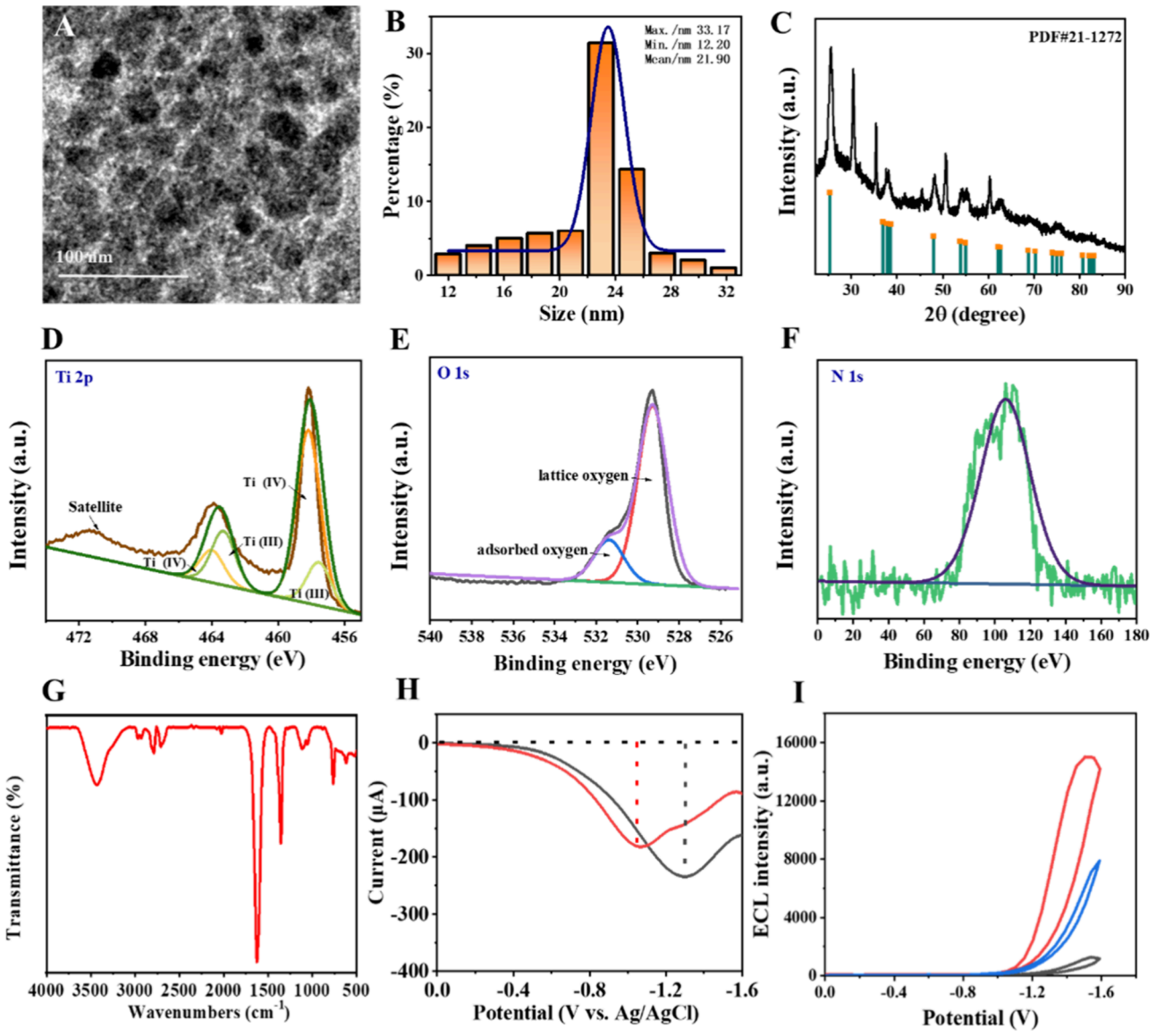

Figure 4. TEM image (A) and particle size distribution diagram (B) of C-TiO_2. XRD pattern of C-TiO_2 (C). XPS spectra of Ti 2p (D), O 1s (E), and N 1s (F) of C-TiO_2. Infrared spectrum of C-TiO_2 (G). DPV curve of C-TiO_2/GCE (black curve) and GCE (red curve) in 0.1 M pH 7.4 PBS containing 0.1 M $K_2S_2O_8$ (H). ECL-potential curve of GCE (black curve), assembled nanoscale Cu NCs sheets/GCE (blue curve), and C-TiO_2/assembled nanoscale Cu NCs sheets/GCE (red curve) in 0.1 M pH 7.4 PBS containing 0.1 M $K_2S_2O_8$ (I).

while the platinum wire electrode serves as the counter electrode (CE). The test solution consists of a PBS solution containing 0.1 M $K_2S_2O_8$. The photomultiplier tube operates at a high voltage setting of 600. The scanning range spans from 0 to −1.60 V, with a scanning rate of 0.50 V/s.

RESULTS AND DISCUSSION

Characterization of Self-Assembled Nanoscale Cu NC Sheets. The morphology of the assembled nanoscale Cu NCs sheets was characterized by using HRTEM (Figure 1A). The self-assembled nanoscale Cu NCs exhibited a well-defined sheet-like structure, with an average length of approximately 200 nm and a width of around 100 nm. The self-assembled nanoscale Cu NCs sheets in Figure 1B exhibit a homogeneous distribution of nanoclusters, characterized by an average particle diameter of 2.18 nm (Figure 1G). The assembled nanoscale Cu NCs sheets underwent Energy dispersive X-ray spectroscopy (EDX) analysis to determine their elemental composition, revealing the presence of Cu, I, S, and C elements (Figure 1H). The mapping results vividly illustrate the distinct outline and homogeneous distribution of Cu, I, and S elements within the assembled nanoscale Cu NCs sheets (Figure 1C∼F). The synthesized assembled nanoscale Cu NCs sheets were subjected to infrared characterization. As shown in Figure 2A, there was no observable characteristic peak of the thiol group at a wavenumber of 2550 cm^{-1}. This finding suggests that dodecanethiol acted as a capping ligand immobilized on the surface through Cu−S bonds. UV−vis spectroscopic analysis revealed that the assembled nanoscale Cu NCs sheets did not have the characteristic surface plasmon resonance absorption peaks typically observed in Cu nanoparticles (Figure 2B), indicating that the nanosheets were composed of Cu NCs. Under excitation at a wavelength of 365 nm, the assembled nanoscale Cu NCs sheets exhibited emission ranging from 544 to 800 nm, with a peak emission observed at 678 nm (Figure 2C). XPS was utilized for the characterization of the valence states of Cu and I.

https://doi.org/10.1021/acs.analchem.4c01039
Anal. Chem. 2024, 96, 7265−7273

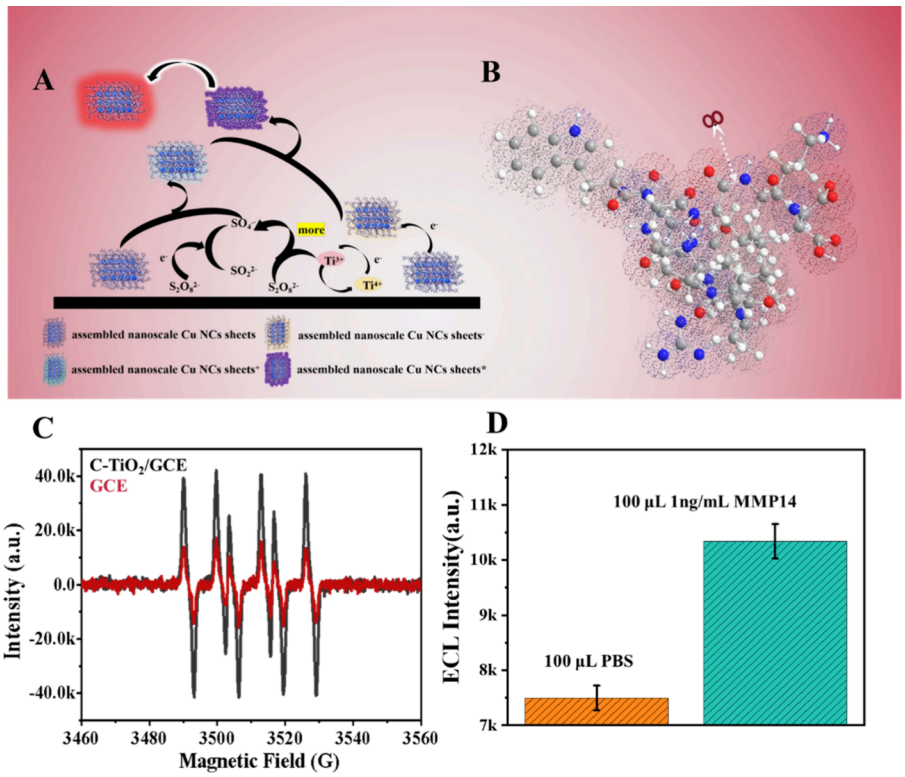

Figure 5. Schematic diagram of the enhanced cathodic ECL mechanism (A) and the cleavage site of MMP 14 for the designed polypeptide chain (B). DMPO spin-trapping EPR spectra of $SO_4^{\cdot-}$ were recorded on different systems under CV tests (C). The viability of MMP 14 sensing strategy testing. Error bars: ± standard deviation (SD), $n = 5$ (D).

In the assembled nanoscale Cu NCs sheets, robust binding energies were observed at 952.3 and 932.4 eV, corresponding to Cu (0) and Cu (I) states. Additionally, XPS results also exhibit a characteristic peak corresponding to Cu (II). A minor shoulder peak at 953.5 eV was observed within the primary peak, indicating the presence of Cu (II) species (Figure 2D). The XPS results unequivocally confirmed the valence state of I (Figure 2E).

A specialized ultrasonic crushing device was used to break the assembled nanoscale Cu NCs into dispersed Cu NCs. Figure 3A presents a TEM image of dispersed Cu NCs. The assembled nanoscale Cu NCs sheets have undergone fragmentation, resulting in a relatively dispersed and irregular morphology. The fluorescence test results demonstrated that ultrasonic fragmentation and dispersion did not induce alteration in the emission wavelength of the Cu NCs. However, under excitation at 365 nm, the dispersed Cu NCs exhibited a significantly diminished intensity of fluorescence at 678 nm (Figure 3B). This phenomenon can be attributed to the tightly and orderly arrangement of Cu NCs, which effectively suppresses surface ligand vibration and rotation, thereby positively contributing to enhancing their fluorescence emission intensity. The ECL of the assembled nanoscale Cu NCs sheets and the dispersed Cu NCs were investigated. It was observed that the ECL intensity of the assembled nanoscale Cu NCs sheets exhibited a 2.99-fold increase compared to that of the dispersed Cu NCs. Furthermore, disparities were observed in onset potential and peak potentials between these two kinds of Cu NCs. Specifically, the dispersed Cu NCs exhibited an ECL onset potential of −1.06 V, accompanied by peak potentials of −1.55 V. In contrast, the assembled nanoscale Cu NCs sheets displayed an ECL onset potential of −0.95 V and reached maximum emission intensity at −1.59 V (Figure 3C). Additionally, the assembled nanoscale Cu NCs sheets exhibited superior luminescence stability with an RSD value of 2.0%. In contrast, the dispersed Cu NCs showed relatively poor ECL stability with a slightly higher RSD value of 3.2% (Figure 3D). We speculate that the self-assembly process leads to a decrease in the specific surface area of the Cu NCs, which indirectly enhances the stability. Consequently, the assembled nanoscale Cu NCs sheets exhibit exceptional ECL stability. The electrochemical properties of the two types of Cu NCs were also investigated. Within a potential scan range of 0 to −1.60 V, the assembled nanoscale Cu NCs sheets gain electrons at −0.49 V, whereas the dispersed Cu NCs displayed a reduction potential at −0.65 V (Figure 3E). The difference in reduction potential implies that the assembled nanoscale Cu NCs sheets are more prone to easier get electrons during the ECL process.

Characterization of C-TiO_2. The TEM of C-TiO_2 revealed that C-TiO_2 is a particulate nanomaterial (Figure 4A), and particle counting from different regions of the sample confirmed the presence of C-TiO_2 particles with an average diameter measuring 21.9 nm (Figure 4B). We have successfully determined the crystal structure of the C-TiO_2 using XRD. Our findings confirm that the C-TiO_2 sample exhibits an anatase phase, with lattice constants measured as $a = 3.785$ Å, $b = 3.785$ Å, and $c = 9.514$ Å, and angles $\alpha = \beta = \gamma = 90°$ (Figure 4C). The surface elemental valence and composition of C-TiO_2 were investigated by XPS analysis. The Ti 2p energy level peaks at 463.3 and 457.6 eV indicate the presence of Ti (III), while peaks at 464.1 and 458.3 eV correspond to Ti (IV) (Figure 4D). The surface of C-TiO_2 exhibits the presence of both adsorbed oxygen and lattice oxygen, as evidenced by peaks at 529.5 eV attributed to lattice oxygen and peaks at 531.4 eV corresponding to

https://doi.org/10.1021/acs.analchem.4c01039
Anal. Chem. 2024, 96, 7265−7273

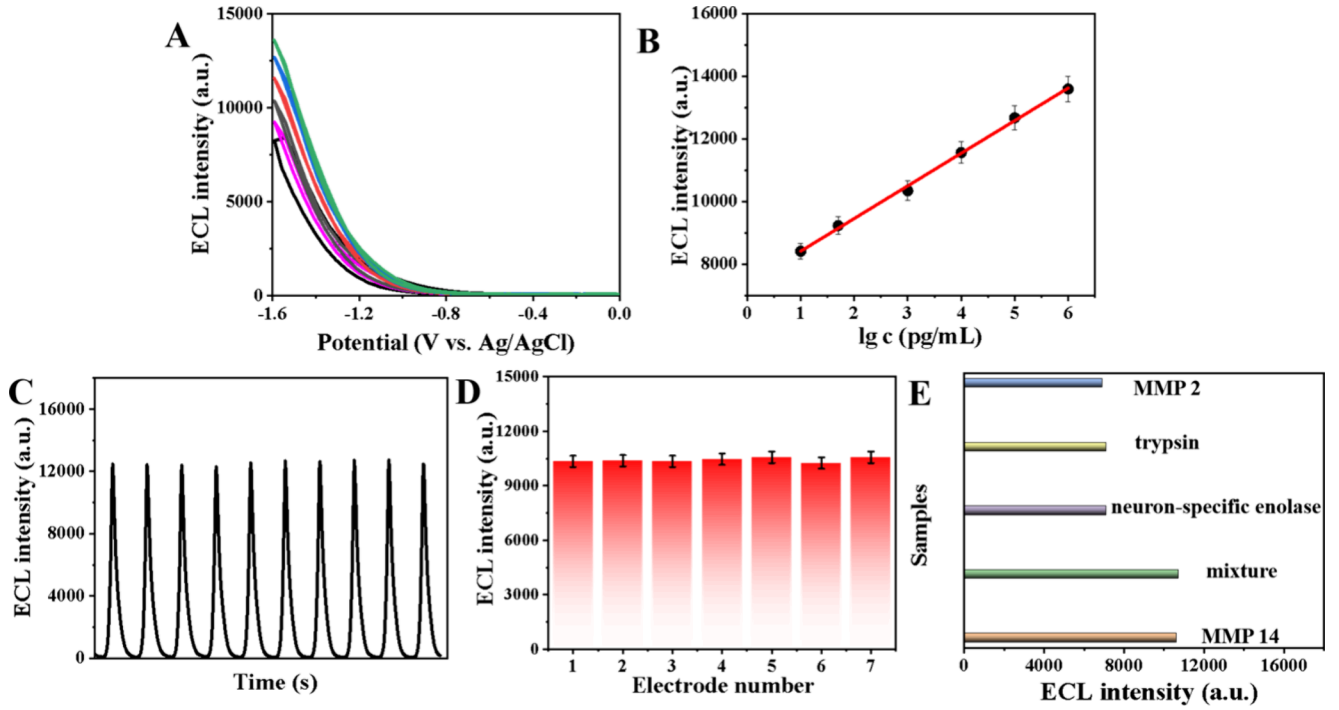

Figure 6. Sensing platform for different concentrations of the MMP 14 signal response (A) and the corresponding calibration curve (B). Test data for sensing platform operational stability (C), reproducibility (D) and selectivity (E). Error bars: ± standard deviation (SD), n = 5 (D).

adsorbed oxygen, respectively (Figure 4E). The successful amination of C-TiO_2 was confirmed by the appearance of the N 1s signal (Figure 4F). Furthermore, the presence of an infrared absorption peak at 3500 to 3300 cm^{-1}, corresponding to the amino groups, provided additional support for the successful amination of C-TiO_2 (Figure 4G). As depicted in Figure 4H, incorporating C-TiO_2 led to an increase in the reduction current for $K_2S_2O_8$, indicating accelerated reaction kinetics for $K_2S_2O_8$ reduction. We investigated the enhancement effect of C-TiO_2 on assembled nanoscale Cu NCs sheets in cathodic ECL and observed that the addition of C-TiO_2 shifted the onset potential of ECL from −0.98 to −0.88 V and the peak potential from −1.59 to −1.51 V, resulting in a significant increase in luminescence intensity by 7123 a.u. (Figure 4I). These results confirm that C-TiO_2 promotes cathodic ECL in $K_2S_2O_8$ of assembled nanoscale Cu NCs sheets.

Enhanced Cathodic ECL Mechanism. Based on the XPS results of C-TiO_2, we propose that the presence of Ti (III) and Ti (IV) in C-TiO_2 plays a pivotal role in enhancing the cathodic ECL of the assembled nanoscale Cu NCs sheets. Combined results of reduction potential tests on $K_2S_2O_8$ and assembled nanoscale Cu NCs sheets (Figure S1), we elucidate an ECL mechanism for the sensing system as follows (Figure 5A): $S_2O_8^{2-}$ gain electron at the electrode surface, leading to the formation of $SO_4^{\cdot-}$ eq 1. Then, a portion of assembled nanoscale Cu NCs sheets reacts with $SO_4^{\cdot-}$, generated at the electrode surface, resulting in assembled nanoscale Cu NCs sheets$^+$ eq 2. Simultaneously, when reaching the reduction potential of assembled nanoscale Cu NCs sheets, the assembled nanoscale Cu NCs sheets gain electrons eq 3. The assembled nanoscale Cu NCs sheets$^+$ subsequently react with assembled nanoscale Cu NCs sheets$^-$, generating an excited state assembled nanoscale Cu NCs sheets eq 4, which then return to their ground state through radiative relaxation eq 5. Reversible cycling between Ti^{4+} and Ti^{3+} in C-TiO_2 can promote the $SO_4^{\cdot-}$ generation, thereby acting as a coreactant promoter eqs 6 and 7. (assembled nanoscale Cu NCs sheets are represented here by Cu NCs).

$$S_2O_8^{2-} + e^- \rightarrow SO_4^{2-} + SO_4^{\cdot-} \quad (1)$$

$$CuNCs + SO_4^{\cdot-} \rightarrow CuNCs^+ + SO_4^{2-} \quad (2)$$

$$CuNCs + e^- \rightarrow CuNCs^- \quad (3)$$

$$CuNCs^+ + CuNCs^- \rightarrow CuNCs^* \quad (4)$$

$$CuNCs^* \rightarrow CuNCs + h\nu \quad (5)$$

$$Ti^{4+} + e^- \rightarrow Ti^{3+} \quad (6)$$

$$Ti^{3+} + S_2O_8^{2-} \rightarrow Ti^{4+} + SO_4^{2-} + SO_4^{\cdot-}(more) \quad (7)$$

Feasibility of Constructing the MMP 14 Sensing Platform. A streptavidin-coated 96-well microplate was utilized for immobilizing Biotin-PLPLRSWGLKD-C-TiO_2. Specific cleavage of Biotin-PLPLRSWGLKD-C-TiO_2 by MMP 14 resulted in the detachment of LKD-C-TiO_2 from the microplate (Figure 5B). The electron-paramagnetic resonance (EPR) results confirmed that C-TiO_2 can promote the generation of more $SO_4^{\cdot-}$ (Figure 5C). Therefore, as LKD-C-TiO_2 detached, the signal of the sensing system increased accordingly. By harnessing the amplification effect of C-TiO_2 on the cathodic ECL response of assembled nanoscale Cu NCs sheets, we successfully achieved a precise determination of the MMP 14 concentration. The sensing system avoids mutual interference and effectively achieves the separation between biological processes and electrode modification. The ECL was employed to characterize the sensor construction process, which demonstrated that replacing 100 μL 1 ng/mL MMP 14 with 100 μL PBS did not cause any significant change in the ECL signal from assembled nanoscale Cu NCs sheets following the operational steps of the sensing platform. After the addition of MMP 14, the short peptide chain was cleaved, leading to an

https://doi.org/10.1021/acs.analchem.4c01039
Anal. Chem. 2024, 96, 7265−7273

Table 1. Results of MMP 14 Determination in Human Serum

original content (ng/mL)	addition content (ng/mL)	average (ng/mL, n = 5)	RSD	recovery
0.53	1.00	1.49	3.8%	96.0%
0.46	0.50	1.00	4.6%	108.0%

augmented signal in the sensing platform due to the detachment of LKD-C-TiO_2 (Figure 5D).

Performance Testing of the Sensing Platform. The ECL signal was recorded at various MMP 14 concentrations to establish a calibration curve. We observed a rise in the ECL signal corresponding to escalating MMP 14 concentrations within the range of 10 to 1,000,000 pg/mL (Figure 6A). The ECL signal demonstrated a linear relationship with the logarithm of MMP 14 concentration, as characterized by the equation I_{ECL} = 1042 logC + 7374, R^2 = 0.999 (Figure 6B). The detection limit was 3.34 pg/mL (S/N = 3). To evaluate operational stability, a 100 ng/mL sample was analyzed for 10 consecutive scan cycles with an RSD of 1.2% at the ECL peak (Figure 6C). The sample containing 1 ng/mL MMP 14 was tested seven times, and the RSD of the seven signal values obtained by the sensing platform was as low as 1.3% (Figure 6D), showing good reproducibility of the sensing platform. In addition, we validated the specificity of the sensing platform using 10 ng/mL of MMP 2, trypsin, and neuron-specific enolase and their mixture as interferences and determined that only 1 ng/mL of MMP 14 could elicit specific responses from the sensing platform, thus confirming its exceptional specificity (Figure 6E).

The precision and reliability of the developed MMP 14 detection platform were evaluated by using the spiked recovery method. The concentration of MMP 14 in two treated serum samples was determined via ELISA, with the addition of different concentrations of MMP 14 standards to the samples. After five assays, the recovery rate fell within the range of 96.0 to 108.0%, with an RSD ranging from 3.8 to 4.6% (Table 1). These results highlight the exceptional precision and reliability of our detection platform.

CONCLUSIONS

In this study, the cathodic ECL intensity and stability of flexible ligand-stabilized Cu NCs were successfully enhanced by employing a self-assembly-induced enhancement strategy. Additionally, by utilizing the facilitation effect of C-TiO_2 on the cathodic ECL of the assembly of nanoscale Cu NCs sheets, we successfully developed a split-type ECL sensing platform for the sensitive detection of MMP 14. The sensing platform leverages the high luminescent properties of assembled nanoscale Cu NCs sheets and the exceptional specificity of short peptides to achieve efficient detection of MMP 14, thereby providing a promising tool for clinical diagnostics and biomedical research.

ASSOCIATED CONTENT

Supporting Information

The Supporting Information is available free of charge at https://pubs.acs.org/doi/10.1021/acs.analchem.4c01039.

DPV curve of assembled nanoscale Cu NCs sheets in 0.1 M pH 7.4 PBS (blue curve) and GCE in 0.1 M pH 7.4 PBS containing 0.1 M $K_2S_2O_8$ (red curve); MMP 14 working curve measured by ELISA (PDF)

AUTHOR INFORMATION

Corresponding Author

Qin Wei − *Key Laboratory of Interfacial Reaction & Sensing Analysis in Universities of Shandong, Collaborative Innovation Center for Green Chemical Manufacturing and Accurate Detection, School of Chemistry and Chemical Engineering, University of Jinan, Jinan 250022, P. R. China; Department of Chemistry, Sungkyunkwan University, Suwon 16419, Republic of Korea;* orcid.org/0000-0002-3034-8046; Email: sdjndxwq@163.com

Authors

Xiaoyue Zhang − *Key Laboratory of Interfacial Reaction & Sensing Analysis in Universities of Shandong, Collaborative Innovation Center for Green Chemical Manufacturing and Accurate Detection, School of Chemistry and Chemical Engineering, University of Jinan, Jinan 250022, P. R. China*

Yue Jia − *Key Laboratory of Interfacial Reaction & Sensing Analysis in Universities of Shandong, Collaborative Innovation Center for Green Chemical Manufacturing and Accurate Detection, School of Chemistry and Chemical Engineering, University of Jinan, Jinan 250022, P. R. China;* orcid.org/0000-0002-2336-4486

Nuo Zhang − *Key Laboratory of Interfacial Reaction & Sensing Analysis in Universities of Shandong, Collaborative Innovation Center for Green Chemical Manufacturing and Accurate Detection, School of Chemistry and Chemical Engineering, University of Jinan, Jinan 250022, P. R. China*

Dan Wu − *Key Laboratory of Interfacial Reaction & Sensing Analysis in Universities of Shandong, Collaborative Innovation Center for Green Chemical Manufacturing and Accurate Detection, School of Chemistry and Chemical Engineering, University of Jinan, Jinan 250022, P. R. China;* orcid.org/0000-0002-8732-5988

Hongmin Ma − *Key Laboratory of Interfacial Reaction & Sensing Analysis in Universities of Shandong, Collaborative Innovation Center for Green Chemical Manufacturing and Accurate Detection, School of Chemistry and Chemical Engineering, University of Jinan, Jinan 250022, P. R. China;* orcid.org/0000-0002-7061-8944

Xiang Ren − *Key Laboratory of Interfacial Reaction & Sensing Analysis in Universities of Shandong, Collaborative Innovation Center for Green Chemical Manufacturing and Accurate Detection, School of Chemistry and Chemical Engineering, University of Jinan, Jinan 250022, P. R. China;* orcid.org/0000-0002-4321-4282

Huangxian Ju − *Key Laboratory of Interfacial Reaction & Sensing Analysis in Universities of Shandong, Collaborative Innovation Center for Green Chemical Manufacturing and Accurate Detection, School of Chemistry and Chemical Engineering, University of Jinan, Jinan 250022, P. R. China; State Key Laboratory of Analytical Chemistry for Life Science, Department of Chemistry, Nanjing University, Nanjing 210023, China;* orcid.org/0000-0002-6741-5302

Complete contact information is available at: https://pubs.acs.org/10.1021/acs.analchem.4c01039

https://doi.org/10.1021/acs.analchem.4c01039
Anal. Chem. 2024, 96, 7265−7273

Notes

The authors declare no competing financial interest.

■ ACKNOWLEDGMENTS

This study was supported by the National Natural Science Foundation of China (nos. 22274062, 22206056), the Natural Science Foundation of Shandong Province (no. ZR2022QB117), and the Special Foundation for Taishan Scholar Professorship of Shandong Province (no. ts20130937).

■ REFERENCES

(1) Zhao, Y.; Descamps, J.; al Hoda Al Bast, N.; Duque, M.; Esteve, J.; Sepulveda, B.; Loget, G.; Sojic, N. *J. Am. Chem. Soc.* **2023**, *145* (31), 17420−17426.
(2) Han, D.; Yang, K.; Sun, S.; Wen, J. *Chem. Eng. J.* **2023**, *476*, No. 146688.
(3) Cho, K. G.; Lee, J. I.; Lee, S.; Hong, K.; Kang, M. S.; Lee, K. H. *Adv. Funct. Mater.* **2020**, *30* (33), No. 1907936.
(4) Liu, Y.; Zhang, H.; Li, B.; Liu, J.; Jiang, D.; Liu, B.; Sojic, N. *J. Am. Chem. Soc.* **2021**, *143* (43), 17910−17914.
(5) Yang, F.; Gong, J.; Li, M.; Jiang, X.; Zhang, J.; Liao, M.; Zhang, H.; Tremblay, P. L.; Zhang, T. *Anal. Chem.* **2023**, *95* (37), 14016−14024.
(6) Zhao, L.; Ren, X.; Ma, H.; Wang, H.; Li, Y.; Wei, Q.; Wu, D.; Ju, H. *Anal. Chem.* **2023**, *95* (36), 13463−13469.
(7) Cheng, M.; Zhang, J.; Huang, T.; Qin, L.; Dong, H.; Liao, F.; Fan, H. *Food Chem.* **2024**, *430*, No. 137030.
(8) Li, H.; Cai, Q.; Xue, Y.; Jie, G. *Biosens. Bioelectron.* **2024**, *245*, No. 115835.
(9) Li, Y.; Gao, X.; Fang, Y.; Cui, B.; Shen, Y. *Coord. Chem. Rev.* **2023**, *485*, No. 215136.
(10) Ma, X.; Gao, W.; Du, F.; Yuan, F.; Yu, J.; Guan, Y.; Sojic, N.; Xu, G. *Acc. Chem. Res.* **2021**, *54* (14), 2936−2945.
(11) Yuan, P. X.; Song, S. S.; Zhan, J.; Chen, C.; Wang, A. J.; Feng, J. J. *Anal. Chem.* **2023**, *95* (50), 18572−18578.
(12) Li, R.; Yang, G.; He, Y.; Zhao, J.; Yuan, R.; Chen, S. *Biosens. Bioelectron.* **2023**, *237*, No. 115539.
(13) Jiang, Q. Q.; Li, Y. J.; Wu, Q.; Wang, X.; Luo, Q. X.; Mao, X. L.; Cai, Y. J.; Liu, X.; Liang, R. P.; Qiu, J. D. *Anal. Chem.* **2023**, *95* (22), 8696−8705.
(14) Yin, B.; Jiang, L.; Wang, X.; Liu, Y.; Kuang, K.; Jing, M.; Fang, C.; Zhou, C.; Chen, S.; Zhu, M. *Aggregate* **2024**, *5*, No. e417.
(15) Wang, D.; Gao, X.; Jia, J.; Zhang, B.; Zou, G. *ACS Nano* **2023**, *17* (1), 355−362.
(16) Chen, S.; Higaki, T.; Ma, H.; Zhu, M.; Jin, R.; Wang, G. *ACS Nano* **2020**, *14* (12), 16781−16790.
(17) Nie, Y.; Tao, X.; Zhou, Y.; Yuan, X.; Zhuo, Y.; Chai, Y. q.; Yuan, R. *Anal. Chem.* **2021**, *93* (2), 1120−1125.
(18) Cui, L.; Zhao, M. h.; Li, C. C.; Wang, Q.; Luo, X.; Zhang, C. Y. *Anal. Chem.* **2021**, *93* (5), 2974−2981.
(19) Zhu, X.; Song, Y.; Wang, X.; Zhou, Y.; Chai, Y.; Yuan, R. *Biosens. Bioelectron.* **2023**, *238*, No. 115580.
(20) Lv, H.; Zhang, R.; Cong, S.; Guo, J.; Shao, M.; Liu, W.; Zhang, L.; Lu, X. *Anal. Chem.* **2022**, *94* (10), 4538−4546.
(21) Xiang, L.; Liu, L. L.; Yuan, R.; Chai, Y. Q. *Anal. Chem.* **2023**, *95* (9), 4454−4460.
(22) Ouyang, X.; Wu, Y.; Guo, L.; Li, L.; Zhou, M.; Li, X.; Liu, T.; Ding, Y.; Bu, H.; Xie, G.; Shen, J.; Fan, C.; Wang, L. *Angew. Chem., Int. Ed.* **2023**, *62* (21), No. e202300893.
(23) Ouyang, X.; Wang, M.; Guo, L.; Cui, C.; Liu, T.; Ren, Y.; Zhao, Y.; Ge, Z.; Guo, X.; Xie, G.; Li, J.; Fan, C.; Wang, L. *Angew. Chem., Int. Ed.* **2020**, *59* (29), 11836−11844.
(24) Liu, Y.; Qi, L.; Li, Z.; Yong, V. W.; Xue, M. *Transl. Stroke Res.* **2023**, DOI: 10.1007/s12975-023-01225-6.
(25) Abdel-Hamid, N. M.; Abass, S. A. *Mol. Biol. Rep.* **2021**, *48* (9), 6525−6538.
(26) Kapoor, C.; Vaidya, S.; Wadhwan, V.; Hitesh; Kaur, G.; Pathak, A. *J. Cancer. Res. Ther.* **2016**, *12* (1), 28−35.
(27) Jin, Y.; Liang, Z. Y.; Zhou, W. X.; Zhou, L. *Pathology* **2020**, *52* (3), 359−365.
(28) Zheng, C. l.; Lu, Q.; Zhang, N.; Jing, P. Y.; Zhang, J. P.; Wang, W. P.; Li, G. Z.; Chen, G. *Dis. Markers* **2021**, *2021*, No. 5917506.
(29) Gonzalez-Molina, J.; Gramolelli, S.; Liao, Z.; Carlson, J. W.; Ojala, P. M.; Lehti, K. *Cells* **2019**, *8* (9), 991.
(30) Li, X.; Li, K.; Li, M.; Lin, X.; Mei, Y.; Huang, X.; Yang, H. *Front. Oncol.* **2022**, *12*, No. 844648.
(31) Liu, Z.; Yao, D.; Ai, L.; Liu, H.; Zhang, S.; Zhang, H. *Soft Matter* **2021**, *17* (17), 4550−4558.
(32) Wang, X.; Gao, P.; Yan, T.; Li, R.; Xu, R.; Zhang, Y.; Du, B.; Wei, Q. *Sens. Actuator, B* **2018**, *258*, 1−9.

https://doi.org/10.1021/acs.analchem.4c01039
Anal. Chem. 2024, 96, 7265−7273